

Protecting K-Nearest Neighbor Queries from Location Inference Attacks

Zhiyu Sun^{1*}, Jie Fu^{2*}, Xinpeng Ling³, Huifa Li⁴, and Zhili Chen¹ (✉)

¹ East China Normal University, China
zhlchen@sei.ecnu.edu.cn

² Stevens Institute of Technology, USA

³ Tongji University, China

⁴ Mohamed bin Zayed University of Artificial Intelligence, UAE

Abstract. The k-nearest neighbor query (kNNQ) is a core component of modern location-based services (LBS) and has been widely adopted in popular features such as “people nearby”. However, its potential privacy risks have long been overlooked. In this work, we present the first two attacks against kNNQ, namely the geometric intersection location inference attack (GI-LIA) and the zero-order optimization location inference attack (ZO-LIA), revealing the inherent location privacy risks posed by kNNQ. To mitigate these privacy risks, we further propose DPRS, a differential privacy framework for kNNQ protection. The core idea of DPRS is to incorporate a rejection sampling mechanism within a constrained perturbation interval, thereby mitigating the distance distortion caused by excessive noise injection. In addition, we design a private interval construction algorithm to construct the perturbation interval, enabling the rejection sampling mechanism to achieve a more favorable trade-off between privacy protection and query utility in kNNQ. Extensive experiments on real-world spatial datasets demonstrate that DPRS outperforms existing methods in both privacy protection and query utility. Our code is available at <https://github.com/reanatom/DPRS>.

Keywords: K-nearest neighbor query · Location inference attack · Differential privacy

1 Introduction

Location-Based Services (LBS) have become a fundamental component of modern mobile applications [14,15,16], but they also introduce significant privacy risks. Prior work has demonstrated that attackers can infer users’ true locations from obfuscated location information. Existing location inference attacks (LIAs) typically exploit distance information [6], spatial regions [23], or user trajectories [21,19] to recover sensitive location data.

* Both authors contributed equally to this work.

However, location privacy threats in k -nearest neighbor query (kNNQ) services (e.g., “nearby people” features) have been largely overlooked. To the best of our knowledge, location inference attacks specifically targeting kNNQ services have not been systematically studied. In such systems, attackers may exploit the ranked neighbor list returned by the API to infer the precise location of a target user. Given the widespread use of kNNQ in social and recommendation applications (such as Tinder [6]), this work systematically investigates location privacy risks in kNNQ services and proposes an effective defense mechanism to mitigate such threats.

Attack design and evaluation. We propose two location inference attacks against kNNQ services: the *Geometric Intersection-based LIA* (GI-LIA) and the *Zero-order Optimization-based LIA* (ZO-LIA). GI-LIA leverages distance relationships between the attacker at multiple query locations and the target, and solves the target’s coordinates using geometric intersection. In contrast, ZO-LIA estimates a pseudo-gradient from the target’s ranking information in query results and iteratively approximates the target’s true location. Experimental results demonstrate that both attacks are highly effective, achieving inference success rates above 95%. These findings indicate that current kNNQ services face severe privacy risks even when users’ exact coordinates are not explicitly disclosed.

Design of defense method. To mitigate location privacy risks in kNNQ, we propose *DPRS*, a privacy-preserving perturbation framework. DPRS perturbs original location data within a carefully constructed privacy region, thereby reducing distance distortion among nearest neighbors. To achieve this goal, we design a rejection-sampling-based location perturbation mechanism that repeatedly proposes and tests candidate locations within a specified interval to ensure the resulting samples follow the target distribution. This mechanism also constrains perturbed samples within the interval, preventing excessive deviation. Applying rejection sampling to DP-kNNQ poses two key challenges: guaranteeing differential privacy under the altered noise distribution and selecting an appropriate perturbation interval to preserve query utility. To address them, we characterize the post-rejection noise using Rényi divergence and design a private interval construction algorithm that adaptively determines the perturbation interval.

Evaluation. We conduct extensive experiments on two real-world datasets and two synthetic datasets to evaluate the performance of DPRS. The results show that DPRS effectively protects location privacy and significantly reduces privacy leakage. In particular, under a low privacy budget, DPRS reduces the success rates of both GI-LIA and ZO-LIA attacks to below 3%, demonstrating the robustness of the proposed defense. Moreover, under the same privacy budget, DPRS consistently outperforms three state-of-the-art location differential privacy methods [1,7,18] across multiple utility metrics. The main contributions of this paper are summarized as follows:

- We present the first location inference attacks against kNNQ services, exposing serious privacy risks in existing kNN-based location services.

- We propose DPRS, a privacy-preserving framework for kNNQ that achieves a better privacy–utility trade-off through constrained perturbation.
- We establish an RDP-based privacy guarantee for the rejection sampling mechanism and derive its utility bound under the default interval.
- Experiments on two real-world and two synthetic datasets show that DPRS consistently outperforms existing methods in both privacy protection and query utility.

2 Background and Related Work

Existing location inference attacks (LIAs) deduce true locations from obfuscated data using probabilistic models and contextual information [1,21,19,3], but fundamentally rely on access to coordinate data or trajectory. This work explores a more stringent scenario: the LBS only returns an anonymous, ranked list of k -nearest neighbors (kNN) [13]. This operation, known as a k -nearest neighbor query (kNNQ), is a fundamental block in numerous modern applications and is defined as follows:

Definition 1. (K-nearest neighbor query [13]) For a query object $q \in O$ and a query parameter k , the k -nearest neighbor query returns the smallest set $NN_q(k) \subseteq D$ that contains (at least) k objects from the database, satisfying:

$$NN_q(k) = \{o \in D \mid d(o, q) \leq d(o_k, q)\}, \quad (1)$$

where o_k is the k -th closest object to q in the database D .

Although kNNQ seemingly protects privacy by concealing coordinates, its ranked list forms a potent side-channel highly susceptible to location inference. Differential privacy (DP) [5] is currently the gold standard for geolocation protection.

Definition 2. (Differential Privacy [5]). The algorithm A provides (ϵ, δ) -Differential Privacy, if for any two neighboring datasets D and D' that differ in only a single entry, $\forall S \subseteq \text{Range}(A)$, the following holds:

$$\Pr(A(D) \in S) \leq e^\epsilon \times \Pr(A(D') \in S) + \delta. \quad (2)$$

DP, foundationalized by geo-indistinguishability [1], is widely applied in LBS [20,12]. However, existing DP-kNNQ methods suffer from severe flaws: L-SRR [18] can only perform kNNQ by perturbing users to a finite, predefined set of points of interest (POIs). This approach severely distorts the data’s underlying spatial distribution, rendering the dataset unusable for other aggregation analyses. Meanwhile, other methods, such as ReuseKNN [11], provide uneven protection; they only apply perturbation to a small subset of users deemed vulnerable, leaving the broader user population with weaker privacy guarantees. Schemes like FedKNN [22], on the other hand, only perturb each participant’s contribution weight, rendering their security entirely dependent on hardware isolation and

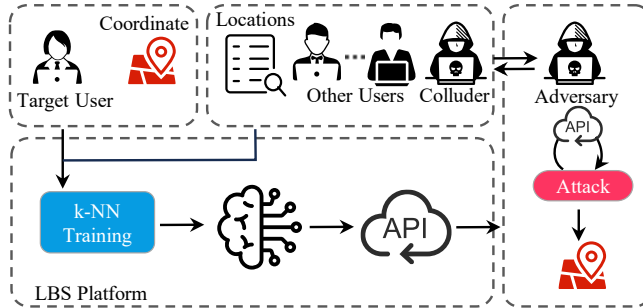


Fig. 1: Threat model

creating a catastrophic “all-or-nothing” privacy risk. To overcome these limitations, we propose the DPRS mechanism. In this paper, we use a more powerful privacy framework: Rényi Differential Privacy (RDP) [10] for privacy loss analysis.

Definition 3. (Rényi Divergence [17]) Given two probability distributions P and Q , the Rényi divergence of order $\alpha > 1$ is:

$$D_\alpha(P\|Q) = \frac{1}{\alpha - 1} \ln \mathbf{E}_{x \sim Q} \left[\left(\frac{P(x)}{Q(x)} \right)^\alpha \right], \quad (3)$$

where $P(x)$, $Q(x)$ denotes the probability density of P , Q .

3 Problem Setup

We consider a location-based service (LBS) platform that maintains a set of users $\mathcal{U} = \{u_1, u_2, \dots, u_N\}$, where each user u_i is associated with a 2D geographic coordinate $L_i = (x_i, y_i)$. The LBS server supports the kNNQ interface that allows a user to submit a query location L_q and obtain a ranked list of the k nearest users based on their distances to L_q . Formally, given a query location L_q , the server returns an ordered list:

$$\text{kNNQ}(L_q) = [u_{(1)}, u_{(2)}, \dots, u_{(k)}]. \quad (4)$$

To protect user privacy, the server does not reveal the exact distance values or the precise locations of users. Instead, it only returns the ranked order of users.

3.1 Threat Model

We consider the adversary who is a legitimate registered user of the LBS platform and has normal access to the kNNQ API. The adversary cannot compromise the server or access its internal data structures, and can only interact with the system through API queries. The adversary possesses the following capabilities:

- **API Access.** The adversary can repeatedly issue kNN queries from arbitrary locations and observe the returned ranked list of anonymized user IDs.
- **Collusion.** The adversary can collaborate with one or more colluding users whose precise locations are known to the adversary. These colluders act as mobile probes that can move to different locations and report their exact coordinates.
- **Adaptive Queries.** The adversary can adaptively change the probe locations and repeatedly query the API to observe how the ranking of the target user changes with respect to other users.

Figure 1 illustrates the threat model. Although the server does not reveal distance values, the ranking output implicitly encodes relative distance information. In particular, when a probe moves to a location where the rank of the target user changes relative to another user, this event indicates that the probe lies on a boundary where the distances to the two users become equal.

Practicality of the Attack. This attack scenario naturally arises in many real-world location-based services. To protect user privacy, many LBS platforms avoid revealing exact locations or distances and instead return a ranked list of nearby users. For example, social applications such as Tinder [6] provide “nearby users” functionality that displays profiles ordered by proximity while hiding precise coordinates or distance values. Since such services are accessible through mobile interfaces or public APIs, an adversary can repeatedly issue queries from different locations—either by moving their own device or collaborating with colluding users, and observe how the target user’s rank changes. These observations enable the adversary to gradually infer the target user’s location.

3.2 Attack Formulation

Let the true location of the target user be $L_t = (x_t, y_t)$. The adversary interacts with the LBS server by issuing a sequence of kNN queries from different probe locations. Let $Q = \{q_1, q_2, \dots, q_n\}$ denotes the set of query results obtained from the server, where each query result q_i corresponds to the ranked list returned by the kNNQ interface at probe location L_i . Meanwhile, the adversary also maintains a set of colluding probe locations $C = \{c_1, c_2, \dots, c_l\}$, where each c_j represents the exact coordinate of a colluder used in the probing process.

Through adaptive probing, the adversary observes the positions where the ranking of the target user changes relative to other users. Based on the collected query results and probe locations, the adversary aims to design a location inference algorithm.

$$\mathcal{A}: (Q, C) \rightarrow L_{inf}, \quad (5)$$

which outputs an estimated location of the target user: $L_{inf} = (x_{inf}, y_{inf})$.

3.3 Measurement of the Attack

To quantitatively evaluate the effectiveness and efficiency of the proposed attack, we adopt three metrics.

Error Distance (Dist). We measure the average inference error between the estimated location and the true location of the target user. Given a set of N attack instances, the average error distance is defined as below:

$$\text{Dist} = \frac{1}{N} \sum_{i=1}^N d(L_{inf}^{(i)}, L_t^{(i)}), \quad (6)$$

where $d(\cdot)$ denotes the Euclidean distance, $L_{inf}^{(i)}$ is the inferred location, and $L_t^{(i)}$ is the true location of the i -th target user.

Attack Success Rate (Acc). We define a successful attack as one where the inferred location lies within a predefined distance threshold τ from the true location. The attack success rate is defined as follows:

$$\text{Acc} = \frac{1}{N} \sum_{i=1}^N \mathbf{1}[d(L_{inf}^{(i)}, L_t^{(i)}) \leq \tau], \quad (7)$$

where $\mathbf{1}[\cdot]$ is the indicator function. In our experimental evaluation, we set $\tau = 100$ meters by default, following the commonly adopted evaluation standard in location privacy research [1].

Attack Cost (Cost). To measure the efficiency of the attack, we compute the average time required to complete an attack instance:

$$\text{Cost} = \frac{1}{N} \sum_{i=1}^N T_i, \quad (8)$$

where T_i denotes the time (seconds) to infer the location of the i -th target user.

Among these metrics, **Dist** and **Acc** reflect the *attack effectiveness*, while **Cost** measures the *attack efficiency*.

4 Our Attack Methods

In this section, we present two attack methods against KNNQ. We first introduce a geometry-based attack and analyze its inherent limitations in terms of communication overhead. We then propose a more communication-efficient attack framework that leverages zeroth-order optimization to achieve a better trade-off between attack effectiveness and efficiency.

4.1 A Straw-man Approach: GI-LIA

The first approach to location inference is based on geometric triangulation. We refer to this baseline method as the Geometric Intersection Location Inference

Attack (GI-LIA). The key idea is to infer the target’s location by determining the intersection points of two circular trajectories on which the target must reside.

First, the attacker establishes an initial circular trajectory centered at an attack point A_1 . Specifically, the attacker determines the radius R_1 of the circle $C(A_1, R_1)$ through a binary search procedure assisted by a collaborator. The collaborator moves radially with respect to A_1 , while the attacker repeatedly issues kNNQ queries. By adjusting the collaborator’s distance from A_1 , the attacker identifies a distance R_1 at which the collaborator’s rank in the query result becomes exactly k . Since the target also appears at rank k , the target must lie on the circumference of $C(A_1, R_1)$.

Next, the attacker selects a second attack point A_2 to obtain another geometric constraint. The attacker performs a search over candidate locations for A_2 , ensuring that (i) A_2 is sufficiently distant from A_1 to provide geometric stability and (ii) the target remains within the kNNQ result set. Once such a point is found, the attacker repeats the binary search procedure to determine the second circular trajectory $C(A_2, R_2)$. The intersection of the two circles $C(A_1, R_1)$ and $C(A_2, R_2)$ yields two candidate locations $\{P_1, P_2\}$. The attacker then issues verification queries at these candidate points and selects the location that yields the lower rank for the target as the inferred target position. The total communication overhead of GI-LIA can be expressed as:

$$Cost_{GI-LIA} = Cost_{binary}^{R_1} + Cost_{search}(A_2) + Cost_{binary}^{R_2} + 2, \quad (9)$$

where $Cost_{binary}$ denotes the query cost of a single binary search used to determine a circle radius, and $Cost_{search}(A_2)$ represents the cost of locating the second attack point A_2 . The final term accounts for the two verification queries at candidate locations P_1 and P_2 . Because both the binary search procedures and the search for A_2 require numerous queries, GI-LIA incurs substantial communication overhead, making it inefficient and impractical for real-time or stealthy attacks.

4.2 Improvement: ZO-LIA

To reduce the excessive communication overhead of GI-LIA, we propose an efficient **zeroth-order optimization location inference attack (ZO-LIA)**. Unlike the GI-LIA, ZO-LIA avoids constructing a second geometric constraint. Instead, it performs a rank-guided local search within the feasible region defined by the first constraint circle and then projects the result onto the circle boundary. The overall process is illustrated in Figure 2.

Phase ①: Radius Search. ZO-LIA first determines the initial constraint circle $C(A_1, R_1)$ using the same radius search procedure described in GI-LIA. By performing a binary search with the help of a collaborator, the attacker finds a distance R_1 such that the collaborator appears at rank k in the kNNQ results. Since the target also appears at rank k , the target must lie on the circumference of $C(A_1, R_1)$.

Phase ②: Probe Generation and Evaluation. Instead of constructing a second circle, ZO-LIA generates a set of probe points around the circle center A_1 .

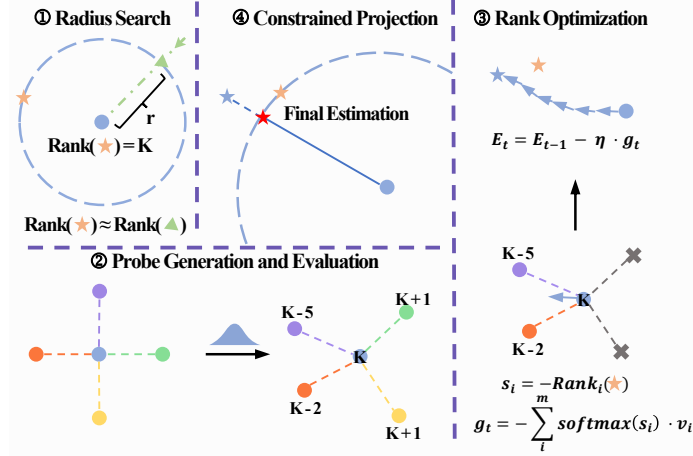


Fig. 2: The framework of ZO-LIA

These probes are sampled along multiple directions in the local neighborhood. For each probe point, the attacker issues a kNNQ query and records the target’s rank. The rank serves as a score indicating how promising the corresponding direction is for approaching the target.

Phase ③: Rank Optimization. This phase constitutes the core of ZO-LIA. We employ a zeroth-order optimization strategy that relies solely on rank feedback. Using the rank scores obtained from the probe evaluations, the attacker estimates a pseudo-gradient that approximates the direction in which the target’s rank decreases most rapidly. The attacker’s position is then iteratively updated along this estimated direction, gradually moving toward an internal point P_{opt} that minimizes the observed rank of the target.

Phase ④: Constrained Projection. Once the search converges to the internal point P_{opt} , a final constrained projection step is applied. Because the target must lie on the circumference of $C(A_1, R_1)$, the attacker orthogonally projects P_{opt} onto the circle boundary. This projection is a simple local computation with constant complexity and produces the final estimate of the target’s location. The total communication overhead of ZO-LIA is given by

$$Cost_{ZO-LIA} = Cost_{binary} + N_{iter} \cdot Cost_{0-iter}, \quad (10)$$

where $Cost_{binary}$ denotes the query cost of the initial radius search, N_{iter} is the number of optimization iterations, and $Cost_{0-iter}$ represents the number of probe queries per iteration.

4.3 Attack performance in real-world scenarios

We evaluate our attacks on two real-world and two synthetic datasets. The evaluation metrics include $Dist$, Acc , and $Cost$ (see §3.3). We consider $k = 10$, $k = 30$,

Table 1: The performance of ZO-LIA and GI-LIA methods across four datasets.

Method	Dataset	k=10			k=30			k=50		
		Dist	Acc	Cost	Dist	Acc	Cost	Dist	Acc	Cost
ZO-LIA	brightkite	28.91	0.948	15.94	40.59	0.914	17.62	41.98	0.912	19.21
	gowalla	39.20	0.960	16.05	56.03	0.906	17.86	56.83	0.926	18.92
	gaussian	24.35	0.956	22.14	42.17	0.910	23.21	43.56	0.893	24.08
	beta	40.39	0.944	22.17	43.96	0.896	23.09	48.51	0.873	23.96
GI-LIA	brightkite	26.93	0.972	31.86	32.67	0.984	33.07	25.74	0.996	35.12
	gowalla	20.59	0.996	31.42	24.55	0.992	34.67	23.56	0.992	35.98
	gaussian	26.31	0.940	44.42	18.34	0.968	45.97	29.98	0.964	48.13
	beta	39.96	0.948	43.21	41.67	0.948	45.07	51.84	0.976	47.31

and $k = 50$. For each k , we perform 5 independent runs with 50 attack instances per run, and report the average results. The results are shown in Table 1. Other attack setups are provided in Appendix A.1.

Attack effectiveness. The results demonstrate that both attacks achieve consistently high effectiveness across all datasets. In particular, both GI-LIA and ZO-LIA maintain success rates above 90% under most settings, indicating that kNNQ-based LBS systems are highly vulnerable to location inference attacks. Among the two methods, GI-LIA achieves the best attack performance. It consistently yields the lowest average distance error and the highest success rates across datasets and k -values. For example, on the Brightkite dataset with $k = 10$, GI-LIA achieves a success rate of 0.972 with an average distance error of only 26.93 meters. These results confirm that the geometric intersection strategy can accurately recover the target’s location.

Attack efficiency. Although GI-LIA achieves the highest attack accuracy, it incurs significantly higher communication overhead. In contrast, ZO-LIA substantially reduces the attack cost while maintaining high success rates. As shown in Table 1, ZO-LIA consistently requires roughly half the execution time of GI-LIA across all datasets and k -values. For instance, on the Brightkite dataset with $k = 30$, the time overhead of ZO-LIA is 17.62 seconds, compared to 33.07 seconds for GI-LIA. This reduction implies fewer queries are needed, making ZO-LIA faster, stealthier, and more practical for real-world attacks.

5 Proposed Defense Method: DPRS

To protect location privacy under kNN queries, we propose the DPRS mechanism. DPRS perturbs the geographic locations in the dataset to produce a new location dataset that strictly satisfies differential privacy guarantees. As illustrated in Figure 3 and Algorithm 3, DPRS consists of two main components: (i) **Private Interval Construction (PIC)**: Establishes a private, data-aware interval for the perturbation. (ii) **Reject Sampling Mechanism (RSM)**: The

Algorithm 1: Private Interval Construction (PIC)

Input: dataset D , sensitivity $2r + 1$, number of clusters m , number of iterations N_c , noise parameter of Lap distribution λ_c , radius scaling γ .

Output: m private centroids.

- 1 Initialize k centroids by initial centroid selection.
- 2 **for** $iter \leftarrow 1$ to N_c **do**
- 3 Get m clusters through the standard k-means.
- 4 Recalculate the centroid of each cluster.
- 5 **for** $j \leftarrow 1$ to m **do**
- 6 **for** $i \leftarrow 1$ to d **do**
- 7 $sum'(C_j^*)[i] = sum(C_j^*)[i] + Lap(0, \lambda_c)$.
- 8 $num'(C_j^*) = num(C_j^*) + Lap(0, \lambda_c)$.
- 9 $c_j = \frac{sum'(C_j^*)}{num'(C_j^*)}$.
- 10 **for** $j \leftarrow 1$ to m **do**
- 11 Find the nearest centroid c_{min} from all centroids excluding c_j .
- 12 $R_j = \gamma \cdot distance(c_j, c_{min})$.
- 13 $I_j = (c_j, R_j)$.
- 14 **return** m private intervals $\{I_1, I_2, \dots, I_m\}$.

core engine that efficiently perturbs data into the private interval constructed by the previous module.

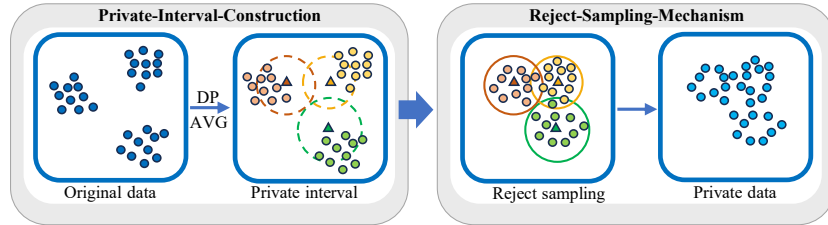


Fig. 3: Overall framework of DPRS

5.1 Private Interval Construction

The privacy interval is designed as a Euclidean ball, consisting of two components: a private center and a private radius. Ideally, to avoid introducing excessive noise offset, the private center should be as close as possible to the original sample. However, directly perturbing the original sample to serve as the interval center would introduce significant distance errors. To address this issue, the DP-k-means algorithm is introduced to obtain more stable and differentially private centers by injecting noise during the aggregation stage. In addition, the private radius is determined by the distance between the two nearest private centers, thereby eliminating the need for additional privacy budget.

Algorithm 2: Rejection Sampling Mechanism (RSM)

Input : data \mathbf{x} , norm n , interval I (center \mathbf{x}_c , radius R), sensitivity $2r$, Lap distribution $p(\cdot|\mathbf{x}, \lambda_p)$, target function $f(\cdot) \propto p(\cdot|\mathbf{x}, \lambda_p)$.

Output: perturbed data \mathbf{x}' .

- 1 **if** $\|\mathbf{x} - \mathbf{x}_c\|_k \leq R$ **then**
- 2 | $M \leftarrow 1$.
- 3 **else**
- 4 | $B \leftarrow \text{GetBoundary}(\mathbf{x}_c, R)$.
- 5 | $\mathbf{z}^* \leftarrow \min_{\mathbf{z} \in B} \|\mathbf{z} - \mathbf{x}\|_n$.
- 6 | $M \leftarrow f(\mathbf{z}^*)$.
- 7 **while** *true* **do**
- 8 | $u, u_1, u_2 \leftarrow \text{RandomUniform}(0, 1)$.
- 9 | $R \leftarrow R\sqrt{u_1}, \theta \leftarrow 2\pi u_2$.
- 10 | $\mathbf{x}' \leftarrow \mathbf{x}_c + (R \cos(\theta), R \sin(\theta))$.
- 11 | **if** $u < \frac{f(\mathbf{x}')}{M}$ **then**
- 12 | | **return** \mathbf{x}' .

As shown in Algorithm 1, PIC is implemented as follows. In each iteration, after samples are assigned to their clusters, the sensitive centroid recomputation step is protected. Specifically, the coordinate sums and the member counts of each cluster are concatenated, and calibrated Laplace noise is injected. The combined operation has a total L_1 sensitivity of $2r + 1$. The private radius of each centroid is then set to half of the distance to its nearest neighboring centroid, which naturally defines the corresponding privacy interval.

5.2 Reject Sampling Mechanism

The rejection sampling mechanism efficiently perturbs private data into the privacy interval constructed by the PIC module. We begin by specifying a base noise distribution, typically $p(\cdot) = \text{Lap}(\cdot | \mathbf{x}, \lambda)$. By normalizing the 2D location data to the range $[-r, r]$, the L_1 sensitivity is bounded by $2r$, which enables calibrated noise injection. To perturb data within the specified Euclidean sphere, we define $f(\cdot) \propto p(\cdot)$, thereby avoiding the computation of the normalization constant. Rejection sampling is then used to generate valid perturbed samples. This procedure requires an upper bound M of $f(\cdot)$ within the sphere in order to compute the acceptance probability. As shown in Algorithm 2 (Lines 1–6), a tight bound M is obtained under either the L_1 norm (Laplace mechanism) or the L_2 norm (Gaussian mechanism) by evaluating a set of candidate points on the boundary of the sphere via $\text{GetBoundary}(\mathbf{x}_c, R)$ (Line 4). Furthermore, we also extend RSM to the Gaussian distribution in Appendix B.

Given these components, the mechanism iteratively performs rejection sampling until a valid sample is accepted. Specifically, a candidate point \mathbf{x}' is first drawn uniformly from the sphere. The acceptance ratio $f(\mathbf{x}')/M$ is then computed, followed by drawing a random variable $u \sim U(0, 1)$. The candidate is

Algorithm 3: Overall algorithm of DPRS

Input : dataset \mathcal{D} , cluster number m , iteration N_c , noise parameter λ_p, λ_c .
Output: perturbed dataset \mathcal{D}' .

- 1 $\{I_1, I_2, \dots, I_k\} \leftarrow \text{PIC}(\mathcal{D}, m, N_c, \lambda_c)$.
- 2 Partition \mathcal{D} into m clusters $\{C_1, C_2, \dots, C_m\}$.
- 3 $\mathcal{D}' \leftarrow \emptyset$.
- 4 **for** $j \leftarrow 1$ **to** m **do**
- 5 **for** $\mathbf{x} \in C_j$ **do**
- 6 $\mathbf{x}' \leftarrow \text{RSM}(\mathbf{x}, I_j, \lambda_p)$.
- 7 $\mathcal{D}' \leftarrow \mathcal{D}' \cup \{\mathbf{x}'\}$.
- 8 **return** \mathcal{D}' .

accepted if $u \leq f(\mathbf{x}')/M$; otherwise, the sample is rejected and the process repeats. Additionally, Theorem 7 and Theorem 8 in the Appendix C.2 guarantee the distributional correctness of the rejection sampling mechanism and provide an upper bound on utility.

6 Privacy Analysis

We first analyze the privacy of the PIC (Algorithm 1) and RSM modules (Algorithm 2), then present the total privacy budget of DPRS (Algorithm 3).

6.1 Privacy Analysis of DPRS Components

Theorem 1. *Algorithm 1 satisfies $(\alpha, \frac{\epsilon_c}{\alpha-1})$ -RDP, where*

$$\epsilon_c = 3N_c \log \left(\frac{\alpha}{2\alpha-1} \exp \left(\frac{\alpha-1}{\lambda_c} \right) + \frac{\alpha-1}{2\alpha-1} \exp \left(\frac{-\alpha}{\lambda_c} \right) \right). \quad (11)$$

Proof. Let D be a dataset partitioned into k disjoint clusters, C_1, \dots, C_k . A neighboring dataset D' is formed by removing a single point, such that $D' = D \setminus \{x\}$ for some $x \in D$, and the partition on D' is composed of clusters C'_1, \dots, C'_k . There exists an index J such that $C'_J = C_J \setminus \{x\}$ and $C'_j = C_j$ elsewhere.

Therefore, each iteration can be regarded as the parallel composition of mechanisms querying function $f(\cdot)$ over k disjoint clusters, and differential privacy achievement is determined by the mechanism over cluster C_J (since mechanisms over other clusters C'_j achieve 0-differential privacy for $C_j = C'_j$).

Let $p(\cdot)$ and $p'(\cdot)$ denote the probability density functions of the mechanism over cluster C_J . For any point $v \in D^{2 \times N}$, its RDP characterization is formed by the composition of three single-dimension Laplace mechanisms, each with a sensitivity of 1, iterated N_c times. The first two mechanisms correspond to the position dimensions, and the last one corresponds to the counting dimension. According to Lemma 1 (§6.2), its privacy characterization is as follows:

$$D_\alpha(p(v)||p'(v)) = \frac{3N_c}{\alpha-1} \log \left(\frac{\alpha}{2\alpha-1} \exp \left(\frac{\alpha-1}{\lambda} \right) + \frac{\alpha-1}{2\alpha-1} \exp \left(-\frac{\alpha}{\lambda} \right) \right). \quad (12)$$

Therefore, Theorem 1 is proved.

Theorem 2. *Algorithm 2 satisfies $(\alpha, \frac{\epsilon_p}{\alpha-1})$ -RDP, where*

$$\epsilon_p = 2 \log \left(\frac{\alpha}{2\alpha-1} \exp \left(\frac{\alpha-1}{\lambda_p} \right) + \frac{\alpha-1}{2\alpha-1} \exp \left(\frac{-\alpha}{\lambda_p} \right) \right). \quad (13)$$

Proof. let $D_\alpha(S)$ be RDP of Algorithm 2, according to Lemma 5 (Appendix C.2) we have:

$$D_\alpha(S) \leq D_\alpha(Lap(\mathbf{t}|\mathbf{0}, \lambda)||Lap(\mathbf{t}|\mu, \lambda)). \quad (14)$$

In fact, the Rényi divergence of the multidimensional Laplace distribution has no analytical expression. Therefore, we characterize the Rényi differential privacy of the multidimensional Laplace distribution as a combination of different dimensions. According to Lemma 1 (§6.2), we have:

$$D_\alpha(Lap(\mathbf{t}|\mathbf{0}, \lambda)||Lap(\mathbf{t}|\mu, \lambda)) = 2D_\alpha(A(0, \lambda)||A(\mu, \lambda)). \quad (15)$$

Therefore, we have:

$$\begin{aligned} D_\alpha(S) &\leq \frac{2}{\alpha-1} \log \int_{-\infty}^{\infty} \left(\frac{1}{2\lambda} e^{-\frac{|x-\mu|}{\lambda}} \right)^\alpha \left(\frac{1}{2\lambda} e^{-\frac{|x|}{\lambda}} \right)^{1-\alpha} dx \\ &= \frac{2}{\alpha-1} \log \left(\frac{1}{2\lambda} \int_{-\infty}^{\infty} \exp \left(-\frac{\alpha|x-\mu| - (\alpha-1)|x|}{\lambda} \right) dx \right) \\ &= \frac{2}{\alpha-1} \log \left(\frac{1}{2\lambda} \left(\int_{-\infty}^0 e^{-\frac{\alpha\mu-x}{\lambda}} dx + \int_0^\mu e^{-\frac{\alpha\mu-(2\alpha-1)x}{\lambda}} dx + \int_\mu^\infty e^{-\frac{x-\alpha\mu}{\lambda}} dx \right) \right) \\ &= \frac{2}{\alpha-1} \log \left(\left(\frac{1}{2} - \frac{1}{2(2\alpha-1)} \right) e^{-\frac{\alpha\mu}{\lambda}} + \left(\frac{1}{2} + \frac{1}{2(2\alpha-1)} \right) e^{\frac{(\alpha-1)\mu}{\lambda}} \right) \\ &= \frac{2}{\alpha-1} \log \left(\frac{\alpha}{2\alpha-1} \exp \left(\frac{(\alpha-1)\mu}{\lambda} \right) + \frac{\alpha-1}{2\alpha-1} \exp \left(-\frac{\alpha\mu}{\lambda} \right) \right). \end{aligned} \quad (16)$$

For single-dimension Laplace noise, it is normalized to the range of $[-1, 1]$, so we set $\mu = 1$. Therefore, Theorem 2 is proved.

Table 2: Statistics of the datasets

Type	Dataset	Locations	Density	Dispersion Index
Real-World	Brightkite [4]	18,409	11.76	0.26%
	Gowalla [4]	17,738	11.33	0.32%
Synthetic	Gaussian [8]	25,000	15.97	0.61%
	Beta [9]	25,000	15.97	0.70%

6.2 Overall Privacy Analysis of DPRS

To derive the total privacy loss, we compose the guarantees from Theorem 1 and 2. This relies on two standard lemmas from the RDP literature:

Lemma 1. (Composition Theorem [10]). *Let two queries f, g be (α, R_1) and (α, R_2) -RDP respectively. Then their composition (f, g) is $(\alpha, R_1 + R_2)$ -RDP.*

Lemma 2. (Conversion Theorem [2]). *If f is an (α, R) -RDP query, then it satisfies $(R + \ln((\alpha - 1)/\alpha) - (\ln \delta + \ln \alpha)/(\alpha - 1), \delta)$ -DP for any $0 < \delta < 1$.*

By applying Lemma 1 to the results of Theorem 1, 2, and then applying Lemma 2, we arrive at the final privacy guarantee for the DPRS framework:

Theorem 3. *Algorithm 3 satisfies $(\epsilon_{Total}, \delta)$ -DP, where*

$$\epsilon_{Total} = \frac{\epsilon_c + \epsilon_p}{\alpha - 1} + \log\left(\frac{\alpha - 1}{\alpha}\right) - \frac{\log(\delta) + \log(\alpha)}{\alpha - 1}. \quad (17)$$

7 Evaluation

In this section, we mainly examine the trade-off between defense effectiveness and KNNQ utility achieved by DPRS and the baselines in the KNNQ task, and further analyze the impact of key parameters on DPRS. There are additional experiment results that can be found in Appendix D.

7.1 Setup

We evaluate DPRS and three baselines (SRR [18], Square [7] and Laplace [1]) on four datasets under various k -NN settings. There are two real-world datasets (Brightkite [4] and Gowalla [4]) and two synthetic datasets (Gaussian [8] and Beta [9]). We restrict the real-world datasets to the San Francisco region, with latitude in $[37.5, 37.9]$ and longitude in $[-122.6, -122.2]$. The synthetic datasets are generated from Gaussian $N(0, 1)$ and Beta $B(2, 5)$ distributions. Dataset details are shown in Table 2. Detailed descriptions of evaluation metrics, baselines, and parameter settings are provided in Appendix A.2.

Table 3: Performance comparison of different defense mechanisms in the 10-NN task. **Recall** and **Ratio** measure query utility, where higher values indicate better query performance. **Acc** and **Dist** characterize the attack performance of ZO-LIA, where lower Acc and higher Dist indicate stronger defense effectiveness.

Dataset	Metric	$\epsilon = 0.5$				$\epsilon = 1$				$\epsilon = 3$				$\epsilon = 5$			
		DPRS	SRR	Square	Laplace	DPRS	SRR	Square	Laplace	DPRS	SRR	Square	Laplace	DPRS	SRR	Square	Laplace
Brightkite	Recall(\uparrow)	0.434	0.382	0.389	0.353	0.464	0.423	0.414	0.398	0.472	0.436	0.440	0.416	0.489	0.447	0.448	0.423
	Ratio(\uparrow)	0.852	0.814	0.811	0.745	0.881	0.832	0.823	0.766	0.885	0.851	0.844	0.699	0.889	0.861	0.856	0.782
	Acc(\downarrow)	0.012	0.016	0.018	0.012	0.014	0.020	0.018	0.016	0.020	0.024	0.018	0.022	0.022	0.028	0.024	0.026
	Dist(\uparrow)	0.591	0.573	0.565	0.594	0.583	0.562	0.553	0.553	0.525	0.516	0.533	0.519	0.524	0.473	0.511	0.515
Gowalla	Recall(\uparrow)	0.443	0.357	0.382	0.331	0.461	0.430	0.418	0.393	0.471	0.453	0.442	0.417	0.482	0.459	0.454	0.446
	Ratio(\uparrow)	0.827	0.773	0.779	0.705	0.872	0.830	0.815	0.737	0.879	0.844	0.840	0.749	0.886	0.853	0.848	0.797
	Acc(\downarrow)	0.022	0.012	0.024	0.018	0.016	0.022	0.022	0.018	0.020	0.022	0.022	0.020	0.020	0.024	0.016	0.018
	Dist(\uparrow)	0.553	0.587	0.544	0.572	0.530	0.481	0.499	0.517	0.517	0.486	0.476	0.497	0.412	0.409	0.476	0.446
Gaussian	Recall(\uparrow)	0.644	0.612	0.587	0.541	0.655	0.637	0.624	0.607	0.664	0.643	0.630	0.611	0.672	0.649	0.645	0.629
	Ratio(\uparrow)	0.902	0.864	0.848	0.792	0.927	0.886	0.874	0.837	0.929	0.888	0.879	0.851	0.933	0.900	0.897	0.863
	Acc(\downarrow)	0.008	0.014	0.018	0.012	0.020	0.016	0.022	0.020	0.014	0.016	0.018	0.018	0.018	0.022	0.020	0.016
	Dist(\uparrow)	0.605	0.587	0.579	0.591	0.547	0.566	0.527	0.533	0.543	0.512	0.504	0.499	0.459	0.423	0.441	0.494
Beta	Recall(\uparrow)	0.563	0.531	0.524	0.482	0.593	0.567	0.553	0.523	0.601	0.582	0.576	0.545	0.623	0.602	0.592	0.594
	Ratio(\uparrow)	0.827	0.751	0.734	0.678	0.861	0.782	0.768	0.714	0.873	0.807	0.796	0.749	0.886	0.822	0.815	0.782
	Acc(\downarrow)	0.012	0.022	0.014	0.018	0.020	0.020	0.022	0.014	0.022	0.024	0.020	0.024	0.016	0.020	0.024	0.016
	Dist(\uparrow)	0.616	0.586	0.608	0.597	0.564	0.553	0.576	0.599	0.512	0.494	0.529	0.481	0.574	0.517	0.483	0.564

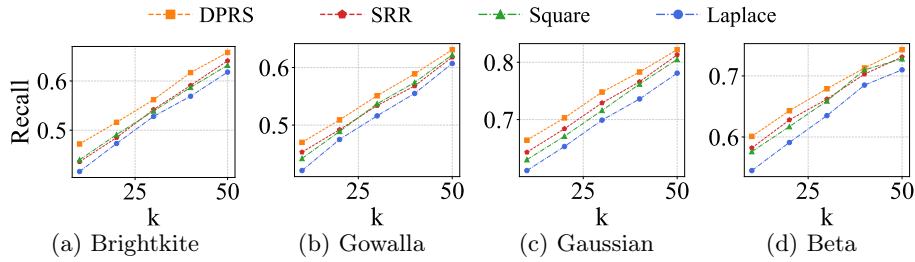
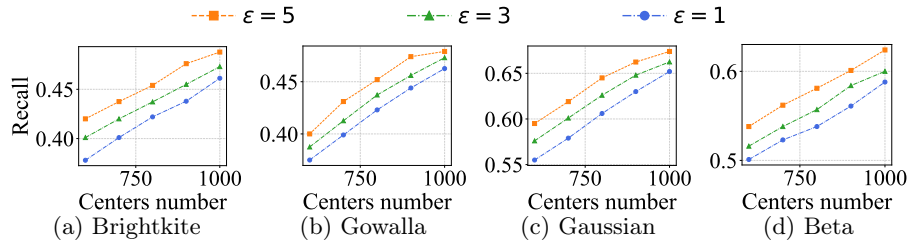
7.2 Tradeoff between Query Utility and Defense Effect

Query utility. As shown in Table 3, DPRS consistently achieves the best query utility across all datasets and privacy budgets. It ranks first in both Recall and Ratio in all 16 settings. Averaged over all settings, DPRS attains a Recall of 0.546 and a Ratio of 0.882, outperforming SRR (0.513/0.835), Square (0.507/0.827), and Laplace (0.482/0.765). Compared with the strongest baseline in each setting, DPRS improves Recall and Ratio by 6.04% and 5.33% on average, respectively. For example, on Brightkite with $\epsilon = 1$, DPRS improves Recall from 0.423 to 0.464 and Ratio from 0.832 to 0.881. On Beta with $\epsilon = 1$, DPRS achieves a Ratio of 0.861, exceeding the best baseline by 0.08.

Defense effect. DPRS also provides strong defense effectiveness against ZO-LIA¹. Averaged over all settings, it achieves the lowest attack success rate (Acc = 0.017) and the largest distance error (Dist = 0.541), compared with 0.020/0.520 for SRR, 0.020/0.525 for Square, and 0.018/0.536 for Laplace. In several cases, DPRS improves both utility and defense simultaneously. For instance, on Brightkite with $\epsilon = 1$, DPRS reduces Acc from 0.02 to 0.014 and increases Dist from 0.562 to 0.583 compared with SRR. On Gaussian with $\epsilon = 3$, DPRS achieves both the lowest Acc (0.014) and the highest Dist (0.543). Although DPRS is not always the best on every single attack metric, it remains highly competitive while preserving substantially better query utility.

Summary. Overall, DPRS achieves the best trade-off between query utility and defense effect. It consistently dominates all baselines in Recall and Ratio, while also achieving the best average defense performance. These results verify that DPRS can effectively protect against location inference attacks without sacrificing kNNQ utility.

¹ As shown in Section 4.3, ZO-LIA achieves the strongest attack performance and is therefore used as the attack baseline.

Fig. 4: Performance impact on the number of neighbors at $\epsilon = 3$.Fig. 5: Performance impact on the number of interval centers at $k = 10$.

7.3 Parameter Sensitivity Analysis

Impact of the Number of Neighbors. We simulated scenarios with k ranging from 10 to 50 on two real-world datasets. As shown in Figure 4, we observe that the query recall consistently increases as the number of neighbors (k) grows. Furthermore, our method consistently outperforms the 2D Laplace, SRR, and Square mechanisms. This further demonstrates that the DPRS framework can effectively preserve the relative distances between neighboring samples.

Impact of the Number of Centers. Figure 5 illustrates the recall performance of our method as the number of interval centers increases from 600 to 1,000. We observe that the recall rate gradually rises with the number of perturbation centers. This is because more centers allow for a more detailed extraction of the dataset’s features, thus capturing neighbor information at a finer granularity.

Impact of the Radius Scaling. The size of the private interval directly determines the utility of the perturbed data, necessitating a careful trade-off for the radius scaling coefficient: An overly large coefficient leads to more frequent overlaps between different clusters, whereas a too small one disrupts the rank differences among nearest neighbors. As shown in Figure 9 in Appendix D, setting the radius scaling coefficient to 0.5 is optimal.

7.4 Time Overhead Analysis

DPRS avoids online query bottlenecks by performing PIC offline and periodically updating private intervals on LBS platforms. Furthermore, as shown in Figure 8

in Appendix D, our RSM incurs only lightweight online overhead given a private interval, which remains below 40ms and is substantially faster than standard noise-and-resampling methods. This demonstrates the scalability of DPRS to large-scale datasets.

8 Conclusion

This work investigates the location privacy issues in kNNQ services. By proposing two attacks, GI-LIA and ZO-LIA, we reveal the privacy threats of kNNQ. To mitigate privacy risk, we propose DPRS, a differentially private framework tailored to high-sensitivity kNNQ. Both theoretical analysis and experimental results show that DPRS can effectively defend against LIA attacks while achieving better utility than state-of-the-art methods.

Acknowledgment

This work is supported by National Natural Science Foundation of China Key Program (Grant No. 62132005), Fundamental Research Funds for the Central Universities (Grant No. 40500-20104-222609).

References

1. Andrés, M.E., Bordenabe, N.E., Chatzikokolakis, K., Palamidessi, C.: Geoindistinguishability: Differential privacy for location-based systems. In: Proceedings of the 2013 ACM SIGSAC conference on Computer & communications security. pp. 901–914 (2013)
2. Balle, B., Barthe, G., Gaboardi, M., Hsu, J., Sato, T.: Hypothesis testing interpretations and renyi differential privacy. In: International Conference on Artificial Intelligence and Statistics. pp. 2496–2506. PMLR (2020)
3. Bitsikas, E., Schnitzler, T., Pöpper, C., Ranganathan, A.: Amplifying threats: The role of multi-sender coordination in sms-timing-based location inference attacks. In: Doupe, A., Milburn, A. (eds.) 18th USENIX WOOT Conference on Offensive Technologies, WOOT 2024, Philadelphia, PA, USA, August 12-13, 2024. pp. 59–73. USENIX Association (2024)
4. Cho, E., Myers, S.A., Leskovec, J.: Friendship and mobility: user movement in location-based social networks. In: Proceedings of the 17th ACM SIGKDD international conference on Knowledge discovery and data mining. pp. 1082–1090 (2011)
5. Dwork, C., Roth, A., et al.: The algorithmic foundations of differential privacy. *Foundations and Trends® in Theoretical Computer Science* **9**(3–4), 211–407 (2014)
6. Frizell, S.: Tinder security flaw exposed users’ locations. *The TIME* (February 2014)
7. Hong, D., Jung, W., Shim, K.: Collecting geospatial data under local differential privacy with improving frequency estimation. *IEEE Transactions on Knowledge and Data Engineering* **35**(7), 6739–6751 (2022)

8. Huang, Z., Liang, Y., Yi, K.: Instance-optimal mean estimation under differential privacy. *Advances in Neural Information Processing Systems* **34**, 25993–26004 (2021)
9. Li, Z., Wang, T., Lopuhaä-Zwakenberg, M., Li, N., Škoric, B.: Estimating numerical distributions under local differential privacy. In: *Proceedings of the 2020 ACM SIGMOD International Conference on Management of Data*. p. 621–635. SIGMOD '20, Association for Computing Machinery, New York, NY, USA (2020)
10. Mironov, I.: Rényi differential privacy. *IEEE Computer Security Foundations Symposium* (2017)
11. Müllner, P., Lex, E., Schedl, M., Kowald, D.: Reuseknn: Neighborhood reuse for differentially private knn-based recommendations. *ACM Transactions on Intelligent Systems and Technology* **14**(5), 1–29 (2023)
12. Niu, B., Chen, Y., Wang, Z., Li, F., Wang, B., Li, H.: Eclipse: Preserving differential location privacy against long-term observation attacks. *IEEE Transactions on Mobile Computing* **21**(1), 125–138 (2020)
13. Seidl, T., Kriegel, H.P.: Optimal multi-step k-nearest neighbor search. In: *Proceedings of the 1998 ACM SIGMOD international conference on Management of data*. pp. 154–165 (1998)
14. Shi, Y., Tong, Y., Zeng, Y., Zhou, Z., Ding, B., Chen, L.: Efficient approximate range aggregation over large-scale spatial data federation. *IEEE Transactions on Knowledge and Data Engineering* **35**(1), 418–430 (2021)
15. Tao, Q., Tong, Y., Zhou, Z., Shi, Y., Chen, L., Xu, K.: Differentially private online task assignment in spatial crowdsourcing: A tree-based approach. In: *2020 IEEE 36th International Conference on Data Engineering (ICDE)*. pp. 517–528. IEEE (2020)
16. Tong, Y., Zhou, Z., Zeng, Y., Chen, L., Shahabi, C.: Spatial crowdsourcing: a survey: Y. tong et al. *The VLDB Journal* **29**(1), 217–250 (2020)
17. Van Erven, T., Harremoës, P.: Rényi divergence and kullback-leibler divergence. *IEEE Transactions on Information Theory* **60**(7), 3797–3820 (2014)
18. Wang, H., Hong, H., Xiong, L., Qin, Z., Hong, Y.: L-srr: Local differential privacy for location-based services with staircase randomized response. In: *Proceedings of the 2022 ACM SIGSAC Conference on computer and communications security*. pp. 2809–2823 (2022)
19. Wang, W., Zhou, X., Qiu, T., He, X., Ge, S.: Location-privacy-aware service migration against inference attacks in multiuser mec systems. *IEEE Internet of Things Journal* **11**(1), 1413–1426 (2023)
20. Wang, Z., Guo, C., Liu, J., Zhang, J., Wang, Y., Luo, J., Yang, X.: Accurate and privacy-preserving task allocation for edge computing assisted mobile crowdsensing. *IEEE Transactions on Computational Social Systems* **9**(1), 120–133 (2021)
21. Yadav, S., Yu, C., Xie, X., Huang, Y., Qiu, C.: Protecting vehicle location privacy with contextually-driven synthetic location generation. In: *Proceedings of the 32nd ACM International Conference on Advances in Geographic Information Systems*. pp. 29–41 (2024)
22. Zhang, X., Wang, Q., Xu, C., Peng, Y., Xu, J.: Fedknn: secure federated k-nearest neighbor search. *Proceedings of the ACM on Management of Data* **2**(1), 1–26 (2024)
23. Zhao, S., Luo, X., Ma, X., Bai, B., Zhao, Y., Zou, W., Yang, Z., Au, M.H., Qiu, X.: Exploiting proximity-based mobile apps for large-scale location privacy probing. *Security and Communication Networks* **2018**(1), 3182402 (2018)

A Experiment Setup

A.1 Experiment Setup of LIA

For the GI-LIA configuration, we set the maximum number of queries for the radius binary search to 100. The center of the second circle (A_2) is determined by generating four surrounding probes. The initial step size for these probes is equal to the radius, with a maximum of 10 retry rounds. If a round fails, the probe generation step size for the subsequent round is reduced by a factor of 0.8.

For the ZO-LIA configuration, which builds upon the GI-LIA settings, we set the number of rank optimization iterations to 10, with 4 probes generated per iteration. Furthermore, we filter out any probes that yield a rank worse than the best result from the previous iteration, thereby preventing them from contributing to the estimation of the current pseudo-gradient direction. The learning rate for this optimization process is set to 0.005.

A.2 Experiment Setup of DPRS

Baseline There are three baselines in our paper: 1) *2D Laplace mechanism* [1]: Perturbs true coordinates by adding noise from a two-dimensional Laplace distribution. 2) *SRR mechanism* [18]: Assigns a staircase of perturbation probabilities to location groups based on their distance from the true coordinates. 3) *Square mechanism* [7]: Employs two distinct probabilities to sample locations, one for a square region around the user and another for the rest of the domain.

Utility Metric For the k-NN task, we use the recall and distance ratio as the utility metrics to evaluate the performance. Given a query point q , the ground truth set is denoted as $G(q)$, and the set returned by the k-NN algorithm is denoted as $P(q)$. The recall and distance ratio are calculated as follows:

$$recall(q, k) = \frac{|P(q) \cap G(q)|}{k}. \quad (18)$$

$$distance\ ratio(q) = \frac{\sum_{g \in G(q)} \|g - q\|_2}{\sum_{p \in P(q)} \|p - q\|_2}. \quad (19)$$

Parameter Settings In our privacy budget design, we set $\epsilon_p = \epsilon_c$ and $\delta = 10^{-5}$. The number of iterations for Algorithm 1 is set to 12. The radius scaling ranges from 0.2 to 0.8 times the initial radius, where the initial radius is defined as the distance from a given center to its nearest center. For location setting, we normalize the data to the range $[-1, 1]$.

B Gaussian Rejection Sampling Mechanism

Algorithm 4 describes the pipeline of applying DPRS to the Gaussian distribution. The main logic aligns with Algorithm 2. The sensitivity of DPRS-Gau is the L_2 norm of the original range (i.e., $\sqrt{2}r$).

C Theoretical Analysis and Proofs

C.1 Theorem for Gaussian Rejection Sampling Mechanism

Algorithm 4: Gaussian-RSM

Input : data \mathbf{x} , interval I (center \mathbf{x}_c , radius R), sensitivity $\|\mu\|_2 = \sqrt{2}r$,
 Gaussian distribution $p(\cdot|\mathbf{x}, \sigma^2 I_d)$, target function $f(\cdot) \propto p(\cdot|\mathbf{x}, \sigma^2 I_d)$.

Output: perturbed data \mathbf{x}' .

```

1 if  $\|\mathbf{x} - \mathbf{x}_c\|_k \leq R$  then
2   |  $M \leftarrow 1$ .
3 else
4   |  $B \leftarrow \text{GetBoundary}(\mathbf{x}_c, R)$ .
5   |  $\mathbf{z}^* \leftarrow \min_{\mathbf{z} \in B} \|\mathbf{z} - \mathbf{x}\|_2$ .
6   |  $M \leftarrow f(\mathbf{z}^*)$ .
7 while true do
8   |  $u, u_1, u_2 \leftarrow \text{RandomUniform}(0, 1)$ .
9   |  $R \leftarrow R\sqrt{u_1}, \theta \leftarrow 2\pi u_2$ .
10  |  $\mathbf{x}' \leftarrow \mathbf{x}_c + (R \cos(\theta), R \sin(\theta))$ .
11  | if  $u < \frac{f(\mathbf{x}')}{M}$  then
12  |   | return  $\mathbf{x}'$ .

```

Theorem 4. Let $p(\mathbf{t}|\mathbf{x}, \sigma^2)$ be a probability density function with support on a bounded domain $D \subset \mathbb{R}^2$, defined as:

$$p(\mathbf{t}|\mathbf{x}, \sigma^2 I_d) = \begin{cases} \frac{1}{N_C} \text{Gau}(\mathbf{t}|\mathbf{x}, \sigma^2 I_d) & \text{if } \mathbf{t} \in D \\ 0 & \text{otherwise,} \end{cases} \quad (20)$$

where $N_C = \iint_D \text{Gau}(\mathbf{t}|\mathbf{x}, \sigma^2 I_d) d\mathbf{t}$. If a sample \mathbf{x}' is generated by Algorithm 4, then the probability distribution of \mathbf{x}' follows distribution $p(\mathbf{t}|\mathbf{x}, \sigma^2 I_d)$.

The detailed proof of Theorem 4 is provided in Theorem 7.

Theorem 5. Algorithm 4 satisfies $(\alpha, \alpha\|\mu\|_2^2/2\sigma^2) - \text{RDP}$.

Proof. let $D_\alpha(S)$ be RDP of Algorithm 4 according to Lemma 5, we have:

$$\begin{aligned}
 D_\alpha(S) &\leq D_\alpha(N(0, \sigma^2 I_d) || N(\mu, \sigma^2 I_d)) \\
 &\leq \frac{1}{\alpha - 1} \log \left\{ \frac{1}{(2\pi\sigma^2)^{d/2}} \cdot \int_{\mathbb{R}^d} \exp \left(-\frac{\alpha \|x - \mu\|_2^2 + (1 - \alpha) \|x\|_2^2}{2\sigma^2} \right) d^d x \right\} \\
 &\leq \frac{1}{\alpha - 1} \log \left\{ \frac{1}{(2\pi\sigma^2)^{d/2}} \cdot \int_{\mathbb{R}^d} \exp \left(-\frac{\alpha(x^T x - 2\mu^T x + \mu^T \mu) + (1 - \alpha)x^T x}{2\sigma^2} \right) d^d x \right\} \\
 &\leq \frac{1}{\alpha - 1} \log \left\{ \frac{1}{(2\pi\sigma^2)^{d/2}} \cdot \int_{\mathbb{R}^d} \exp \left(-\frac{x^T x - 2\alpha\mu^T x + \alpha\|\mu\|^2}{2\sigma^2} \right) d^d x \right\} \\
 &\leq \frac{1}{\alpha - 1} \log \left\{ \frac{1}{(2\pi\sigma^2)^{d/2}} \cdot \int_{\mathbb{R}^d} \exp \left(-\frac{\|x - \alpha\mu\|^2 - \alpha(\alpha - 1)\|\mu\|^2}{2\sigma^2} \right) d^d x \right\} \\
 &\leq \frac{1}{\alpha - 1} \log \left\{ \exp \left(\frac{\alpha(\alpha - 1)\|\mu\|^2}{2\alpha^2} \right) \frac{1}{(2\pi\sigma^2)^{d/2}} \cdot \int_{\mathbb{R}^d} \exp \left(-\frac{\|x - \alpha\mu\|^2}{2\sigma^2} \right) d^d x \right\} \\
 &\leq \frac{\alpha\|\mu\|_2^2}{2\alpha^2}.
 \end{aligned} \tag{21}$$

So, Theorem 5 is proved.

Theorem 6. Let $\mathbf{x}_c = (0, 0)$, $R = 1$. For any input point $\mathbf{x} \in [-1, 1] \times [-1, 1]$, Algorithm 4 produces a perturbed output $\mathbf{x}' = A(\mathbf{x})$. Then the expected distance between \mathbf{x} and \mathbf{x}' is bounded as follows:

$$\mathbb{E}_A[\|x' - x\|] \leq \sigma \sqrt{\frac{2}{\pi}} \cdot \frac{1 - e^{-\frac{2}{\sigma^2}}}{\Phi\left(\frac{2}{\sigma}\right) - \frac{1}{2}}. \tag{22}$$

Proof. In fact, no analytical solution exists for the rejection sampling mechanism on the unit disk. Therefore, we replace the perturbation interval with a square region $S = [-1, 1]^2$. In fact, we have:

$$E_A[\|x - x'\|_1] \leq \frac{\iint_S \|y - x\|_1 \exp\left(-\frac{\|y-x\|_2^2}{2\sigma^2}\right) dy}{\iint_S \exp\left(-\frac{\|y-x\|_2^2}{2\sigma^2}\right) dy} = \frac{N_{2D}(x)}{C_{2D}(x)}. \tag{23}$$

$$\begin{aligned}
 C_{2D}(x) &= \int_{-1}^1 \int_{-1}^1 \exp\left(-\frac{(y_1 - x_1)^2}{2\sigma^2}\right) \exp\left(-\frac{(y_2 - x_2)^2}{2\sigma^2}\right) dy_1 dy_2 \\
 &= \left(\int_{-1}^1 \exp\left(-\frac{(t - x_1)^2}{2\sigma^2}\right) dt \right) \cdot \left(\int_{-1}^1 \exp\left(-\frac{(t - x_2)^2}{2\sigma^2}\right) dt \right) \\
 &= C_{1D}(x_1) \cdot C_{1D}(x_2).
 \end{aligned} \tag{24}$$

$$\begin{aligned}
N_{2D}(x) &= \iint_S (|y_1 - x_1| + |y_2 - x_2|) \exp\left(-\frac{\|y - x\|_2^2}{2\sigma^2}\right) dy \\
&= \iint_S |y_1 - x_1| \exp(-\dots) dy + \iint_S |y_2 - x_2| \exp(-\dots) dy \\
&= \left(\int_{-1}^1 |t - x_1| e^{-\frac{(t-x_1)^2}{2\sigma^2}} dt\right) \cdot \left(\int_{-1}^1 e^{-\frac{(t-x_2)^2}{2\sigma^2}} dt\right) \\
&\quad + \left(\int_{-1}^1 |t - x_2| e^{-\frac{(t-x_2)^2}{2\sigma^2}} dt\right) \cdot \left(\int_{-1}^1 e^{-\frac{(t-x_1)^2}{2\sigma^2}} dt\right) \\
&= N_{1D}(x_1)C_{1D}(x_2) + N_{1D}(x_2)C_{1D}(x_1).
\end{aligned} \tag{25}$$

$$\begin{aligned}
E_A[|x - x'|_1] &\leq \frac{N_{1D}(x_1)C_{1D}(x_2) + C_{1D}(x_1)N_{1D}(x_2)}{C_{1D}(x_1)C_{1D}(x_2)} \\
&= \frac{N_{1D}(x_1)}{C_{1D}(x_1)} + \frac{N_{1D}(x_2)}{C_{1D}(x_2)}.
\end{aligned} \tag{26}$$

Let $E_{1D}(x) = \frac{N_{1D}(x)}{C_{1D}(x)}$, in fact we have:

$$\begin{aligned}
E_{1D}(x) \leq E_{1D}(1) &= \frac{\int_{-1}^1 |y - 1| \exp\left(-\frac{(y-1)^2}{2\sigma^2}\right) dy}{\int_{-1}^1 \exp\left(-\frac{(t-1)^2}{2\sigma^2}\right) dt} \\
&= \frac{\int_{-2}^0 |z| \exp\left(-\frac{z^2}{2\sigma^2}\right) dz}{\int_{-2}^0 \exp\left(-\frac{z^2}{2\sigma^2}\right) dz} \\
&= \frac{\sigma^2 \left(1 - e^{-2/\sigma^2}\right)}{\sigma \int_{-2/\sigma}^0 e^{-t^2/2} dt} \\
&= \frac{\sigma \left(1 - e^{-2/\sigma^2}\right)}{\sqrt{2\pi} (\Phi(2/\sigma) - 1/2)}.
\end{aligned} \tag{27}$$

Therefore, Theorem 6 is proved as follows:

$$E_A[|x - x'|_1] \leq 2E_{1D}(x) \leq \sigma \sqrt{\frac{2}{\pi}} \cdot \frac{1 - e^{-\frac{2}{\sigma^2}}}{\Phi\left(\frac{2}{\sigma}\right) - \frac{1}{2}}. \tag{28}$$

C.2 Lemma and Theorem for Laplace Rejection Sampling Mechanism

Lemma 3. For any interval S and $\alpha > 1$, we have:

$$I_\alpha(S) \cdot Z_Q(S)^{\alpha-1} \geq Z_P(S)^\alpha, \tag{29}$$

where $I_\alpha(S) = \int_S p(x)^\alpha q(x)^{1-\alpha} dx$, $Z_P(S) = \int_S p(x) dx$, $Z_Q(S) = \int_S q(x) dx$.

Proof. we define $g(x) = \frac{q(x)}{Z_Q(S)}$, $h(x) = \frac{p(x)}{q(x)}$ and a convex function $f(t) = t^\alpha$.

Definition 4 (Jensen's Inequality). If $f(\cdot)$ is a convex function, then for any $g(x)$, $h(x)$, we have:

$$f\left(\int h(x)g(x)dx\right) \leq \int f(h(x))g(x)dx. \quad (30)$$

According to Definition 4 above, we have:

$$\begin{aligned} f\left(\int_S h(x)g(x)dx\right) &\leq \int_S f(h(x))g(x)dx \\ \iff f\left(\int_S \frac{p(x)}{q(x)} \frac{q(x)}{Z_Q(S)} dx\right) &\leq \int_S \left(\frac{p(x)}{q(x)}\right)^\alpha \frac{q(x)}{Z_Q(S)} dx \\ \iff f\left(\frac{1}{Z_Q(S)} \int_S p(x)dx\right) &\leq \frac{1}{Z_Q(S)} \int_S p(x)^\alpha q(x)^{1-\alpha} dx \\ \iff \left(\frac{Z_P(S)}{Z_Q(S)}\right)^\alpha &\leq \frac{I_\alpha(S)}{Z_Q(S)} \\ \iff I_\alpha(S) \cdot Z_Q(S)^{\alpha-1} &\geq Z_P(S)^\alpha. \end{aligned} \quad (31)$$

So Lemma 3 is proved.

Lemma 4. for any $x, y > 0$ and $\alpha > 1$, we have:

$$(1+x)^\alpha(1+y)^{1-\alpha} - x^\alpha y^{1-\alpha} \leq 1. \quad (32)$$

Proof. we define $g(x) = (1+x)^\alpha(1+y)^{1-\alpha} - x^\alpha y^{1-\alpha}$, we have:

$$\begin{aligned} g'(x) &= \alpha(1+x)^{\alpha-1}(1+y)^{1-\alpha} - \alpha x^{\alpha-1} y^{1-\alpha} \\ \text{let } g'(x) &= 0 \\ \iff \alpha(1+x)^{\alpha-1}(1+y)^{1-\alpha} &= \alpha x^{\alpha-1} y^{1-\alpha} \\ \iff \left(\frac{1+x}{x}\right)^{\alpha-1} &= \left(\frac{1+y}{y}\right)^{\alpha-1} \\ \iff x &= y. \end{aligned} \quad (33)$$

When $x > y$, $g'(x) < 0$; when $x < y$, $g'(x) > 0$ So we have:

$$\begin{aligned} g(x) \leq g(y) &= (1+y)^\alpha(1+y)^{1-\alpha} - y^\alpha y^{1-\alpha} \\ &= (1+y)^\alpha - y^\alpha \\ &= 1. \end{aligned} \quad (34)$$

so, Lemma 4 is proved.

Lemma 5. let $D_\alpha(S) = \frac{1}{\alpha-1} \log\left(\frac{I_\alpha(S)}{Z_P(S)^\alpha Z_Q(S)^{1-\alpha}}\right)$, if $S_1 \subseteq S_2$, then $D_\alpha(S_1) \leq D_\alpha(S_2)$. where $I_\alpha(S) = \int_S p(x)^\alpha q(x)^{1-\alpha} dx$, $Z_P(S) = \int_S p(x) dx$, $Z_Q(S) = \int_S q(x) dx$.

Proof. let $S_2 = S_1 \cup S_{rem}$, we can prove this as follows:

$$\begin{aligned}
D_\alpha(S_1) &\leq D_\alpha(S_2) \\
\iff \frac{I_\alpha(S_1)}{Z_P(S_1)^\alpha Z_Q(S_1)^{1-\alpha}} &\leq \frac{I_\alpha(S_2)}{Z_P(S_2)^\alpha Z_Q(S_2)^{1-\alpha}} \\
\iff \left(\frac{Z_P(S_2)}{Z_P(S_1)}\right)^\alpha \left(\frac{Z_Q(S_2)}{Z_Q(S_1)}\right)^{1-\alpha} &\leq \frac{I_\alpha(S_2)}{I_\alpha(S_1)} \\
\iff \left(1 + \frac{Z_P(S_{rem})}{Z_P(S_1)}\right)^\alpha \left(1 + \frac{Z_Q(S_{rem})}{Z_Q(S_1)}\right)^{1-\alpha} &\leq 1 + \frac{I_\alpha(S_{rem})}{I_\alpha(S_1)}.
\end{aligned} \tag{35}$$

According to Lemma 3 we have:

$$\begin{aligned}
I_\alpha(S_{rem}) \cdot Z_Q(S_{rem})^{\alpha-1} &\geq Z_P(S_{rem})^\alpha \\
I_\alpha(S_1) \cdot Z_Q(S_1)^{\alpha-1} &\geq Z_P(S_1)^\alpha \\
\iff \frac{I_\alpha(S_{rem})}{I_\alpha(S_1)} &\geq \left(\frac{Z_P(S_{rem})}{Z_P(S_1)}\right)^\alpha \cdot \left(\frac{Z_Q(S_{rem})}{Z_Q(S_1)}\right)^{1-\alpha}.
\end{aligned} \tag{36}$$

So, let $x = \frac{Z_P(S_{rem})}{Z_P(S_1)}$, $y = \frac{Z_Q(S_{rem})}{Z_Q(S_1)}$, we need to prove

$$1 + x^\alpha y^{1-\alpha} \geq (1+x)^\alpha (1+y)^{1-\alpha}. \tag{37}$$

According to Lemma 4, Lemma 5 is proved.

Theorem 7. Let $p(\mathbf{t}|\mathbf{x}, \lambda)$ be a probability density function with support on a bounded domain $D \subset \mathbb{R}^2$, defined as:

$$p(\mathbf{t}|\mathbf{x}, \lambda) = \begin{cases} \frac{1}{N_C} \text{Lap}(\mathbf{t}|\mathbf{x}, \lambda) & \text{if } \mathbf{t} \in D \\ 0 & \text{otherwise,} \end{cases} \tag{38}$$

where $N_C = \iint_D \text{Lap}(\mathbf{t}|\mathbf{x}, \lambda) d\mathbf{t}$.

If a sample \mathbf{x}' is generated by Algorithm 2, then the probability distribution of \mathbf{x}' follows target distribution $p(\mathbf{t}|\mathbf{x}, \lambda)$.

Proof. To prove Theorems 4 and Theorems 7, we need to establish a more general result from which they follow. let noisy distribution be $p(x)$ as follows:

$$p(\mathbf{x}) = \begin{cases} \frac{1}{N_C} f^*(\mathbf{x}) & \text{if } \mathbf{x} \in D \\ 0 & \text{otherwise,} \end{cases} \tag{39}$$

where $N_C = \int_D f^*(\mathbf{z}) d\mathbf{z}$ is the normalization constant.

we assume D is a Euclidean sphere with a radius R and Y is the output of RSM. We will prove that $\Pr[Y = x|\text{accept}] = p(x)$, in fact, we have:

$$\begin{aligned}
\Pr[Y = x|\text{accept}] &= \frac{\Pr[\text{accept}|Y = x] \cdot \Pr[Y = x]}{\Pr[\text{accpet}]} \\
&= \frac{\Pr[\text{accept}|Y = x] \cdot \frac{1}{\pi R^2}}{\Pr[\text{accpet}]}.
\end{aligned} \tag{40}$$

For the first term in the numerator, we can calculate it in the following way:

$$\Pr[\text{accept}|Y = x] = \Pr[u < \frac{f^*(x)}{M}] = \frac{f^*(x)}{M}, \quad (41)$$

where M is the max probability value in D , and $u \sim \text{Uniform}(0, 1)$.

For the denominator, we can calculate it in the following manner:

$$\begin{aligned} \Pr[\text{accept}] &= \int_{x \in D} \Pr[\text{accept}|Y = x] \cdot \Pr[Y = x] dx \\ &= \int_{x \in D} \frac{f^*(x)}{M} \cdot \frac{1}{\pi R^2} dx \\ &= \frac{\int_{x \in D} f^*(x) dx}{M\pi R^2} \\ &= \frac{N_c}{M\pi R^2}. \end{aligned} \quad (42)$$

So, we have:

$$\begin{aligned} \Pr[Y = x|\text{accept}] &= \frac{\Pr[\text{accept}|Y = x] \cdot \frac{1}{\pi R^2}}{\Pr[\text{accept}]} \\ &= \frac{f^*(x)}{M} \cdot \frac{1}{\pi R^2} \cdot \frac{M\pi R^2}{N_c} \\ &= \frac{f^*(x)}{N_c} \\ &= p(x). \end{aligned} \quad (43)$$

Therefore, Theorem 4 and Theorem 7 are proved.

Theorem 8. Let $\mathbf{x}_c = (0, 0)$, $R = 1$. For any input point $\mathbf{x} \in [-1, 1] \times [-1, 1]$, Algorithm 2 produces a perturbed output $\mathbf{x}' = A(\mathbf{x})$. Then the expected distance between \mathbf{x} and \mathbf{x}' is bounded as follows:

$$\mathbb{E}_A[\|\mathbf{x}' - \mathbf{x}\|_1] \leq 2(\lambda - \frac{2}{e^{2/\lambda} - 1}). \quad (44)$$

Proof. In fact, the rejection sampling mechanism on the unit circle has no analytical solution. For this reason, we choose to calculate the expectation of the analytical expression on a square region $S = [-1, 1]^2$, because the region S is slightly larger than the unit circle, from which an upper bound can be obtained:

$$E_A[\|x - x'\|_1] \leq \frac{\iint_S \|y - x\|_1 \exp(-\frac{\|y-x\|_1}{\lambda}) dy}{\iint_S \exp(-\frac{\|y-x\|_1}{\lambda}) dy}. \quad (45)$$

Let $C_{2D}(x) = \iint_S \|y - x\|_1 \exp(-\frac{\|y-x\|_1}{\lambda}) dy$, we have:

$$\begin{aligned} C_{2D}(x) &= \int_{-1}^1 \int_{-1}^1 \exp\left(-\frac{|y_1 - x_1|}{\lambda}\right) \exp\left(-\frac{|y_2 - x_2|}{\lambda}\right) dy_1 dy_2 \\ &= \left(\int_{-1}^1 \exp\left(-\frac{|t - x_1|}{\lambda}\right) dt\right) \cdot \left(\int_{-1}^1 \exp\left(-\frac{|t - x_2|}{\lambda}\right) dt\right) \\ &= C_{1D}(x_1) \cdot C_{1D}(x_2). \end{aligned} \quad (46)$$

Let $N_{2D}(x) = \iint_S \exp(-\frac{\|y-x\|_1}{\lambda}) dy$, we have:

$$\begin{aligned} N_{2D}(x) &= \iint_S \left(\sum_i |y_i - x_i|\right) H_i \exp\left(-\frac{|y_i - x_i|}{\lambda}\right) dy_1 dy_2 \\ &= \left(\int_{-1}^1 |y_1 - x_1| e^{-\frac{|y_1 - x_1|}{\lambda}} dy_1\right) \cdot \left(\int_{-1}^1 e^{-\frac{|y_2 - x_2|}{\lambda}} dy_2\right) \\ &\quad + \left(\int_{-1}^1 e^{-\frac{|y_2 - x_2|}{\lambda}} dy_2\right) \cdot \left(\int_{-1}^1 |y_1 - x_1| e^{-\frac{|y_1 - x_1|}{\lambda}} dy_1\right) \\ &= N_{1D}(x_1) C_{1D}(x_2) + C_{1D}(x_1) N_{1D}(x_2). \end{aligned} \quad (47)$$

Hence, the original formula is represented as follows:

$$\begin{aligned} E_A[|x - x'|_1] &\leq \frac{N_{1D}(x_1) C_{1D}(x_2) + C_{1D}(x_1) N_{1D}(x_2)}{C_{1D}(x_1) C_{1D}(x_2)} \\ &= \frac{N_{1D}(x_1)}{C_{1D}(x_1)} + \frac{N_{1D}(x_2)}{C_{1D}(x_2)}. \end{aligned} \quad (48)$$

Let $E_{1D}(x) = \frac{N_{1D}(x)}{C_{1D}(x)}$, in fact we have:

$$\begin{aligned} E_{1D}(x) &\leq E_{1D}(1) = \frac{\int_{-1}^1 |y - 1| \exp\left(-\frac{|y-1|}{\lambda}\right) dy}{\int_{-1}^1 \exp\left(-\frac{|t-1|}{\lambda}\right) dt} \\ &= \frac{\int_2^0 z e^{-z/\lambda} (-dz)}{\int_2^0 e^{-z/\lambda} (-dz)} \\ &= \frac{\lambda^2 - \lambda(\lambda + 2)e^{-2/\lambda}}{\lambda(1 - e^{-2/\lambda})} \\ &= \lambda - \frac{2}{e^{2/\lambda} - 1}. \end{aligned} \quad (49)$$

Therefore, Theorem 8 is proved as follows:

$$E_A[|x - x'|_1] \leq 2E_{1D}(x) \leq 2\left(\lambda - \frac{2}{e^{2/\lambda} - 1}\right). \quad (50)$$

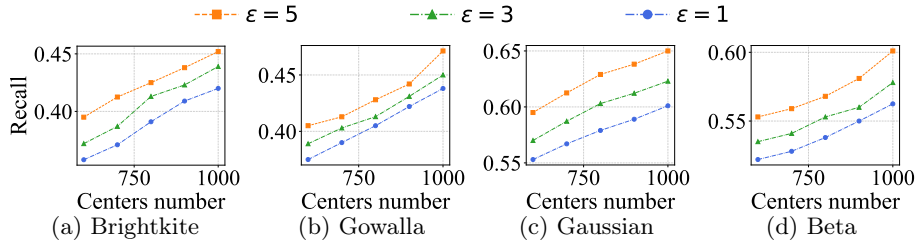


Fig. 6: Performance impact on the number of interval centers for DPRS-Gau in 10-NN task at $k = 10$.

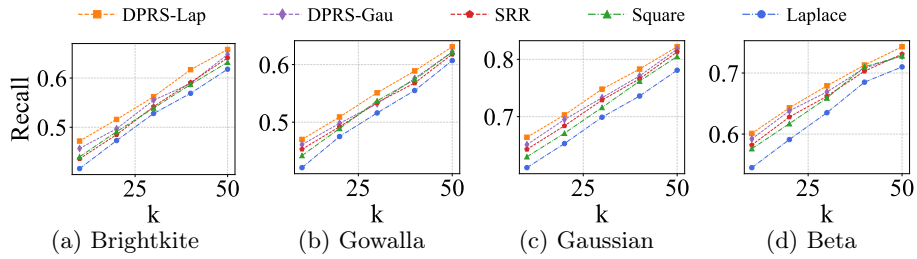


Fig. 7: Performance impact on the number of neighbors for all mechanisms in the 10-NN task at $\epsilon = 3$.

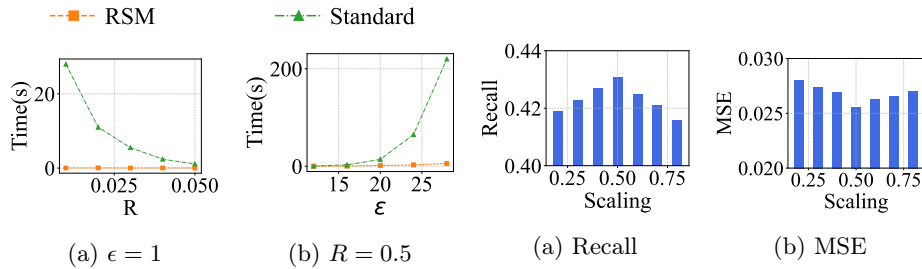


Fig. 8: Time overhead for sampling algorithms.

Fig. 9: Performance impact on radius scaling selection.

D Additional Experiment Results

Experiments of RSM-Gau. Figures 6 and 7 demonstrate the performance of integrating RSM-Gau into DPRS. Specifically, the former shows that the recall of DPRS-Gau increases as the number of centers grows from 600 to 1000 and larger privacy budgets (ϵ) also yield higher recall, while the latter indicates that both DPRS-Gau and DPRS-Lap outperform the baselines (SRR, Square, and Laplace) across all datasets, confirming the effectiveness of the DPRS framework.

Time overhead analysis of DPRS. We set the interval center to $(0, 0)$ and uniformly sample 100 samples from the square $[-1, 1] \times [-1, 1]$, then compare the time cost of perturbing these samples into the interval. As shown in Figure 8, compared to the standard noise-and-resampling mechanism, our RSM consistently maintains a minimal time overhead (less than 40ms) under varying radius (R) and privacy budget (ϵ) settings.

Optimal τ Analysis. We evaluate the perturbation radius scaling at $\epsilon = 1$. Figure 9 illustrates the impact of varying the scaling coefficient on k -NN recall and distance MSE. Specifically, setting the radius to 0.5 times the distance to the nearest PIC center yields the optimal performance, achieving the highest recall and the lowest MSE.